ACS APPLIED MATERIALS & INTERFACES

Research Article

www.acsami.org

Surface Wettability of Macroporous Anodized Aluminum Oxide

Josephus G. Buijnsters,*[,†] Rui Zhong,[†] Natalia Tsyntsaru,[†,‡] and Jean-Pierre Celis[†]

[†]Department of Metallurgy and Materials Engineering, KU Leuven, Kasteelpark Arenberg 44, B-3001 Leuven, Belgium

[‡]Institute of Applied Physics of Academy of Sciences of Moldova, 5 Academy Strasse, Chisinau, MD - 2028, Moldova

Supporting Information

ABSTRACT: The correlation between the structural characteristics and the wetting of anodized aluminum oxide (AAO) surfaces with large pore sizes (>100 nm) is discussed. The roughness-induced wettability is systematically examined for oxide films grown by a two-step, high-field anodization in phosphoric acid of three different concentrations using a commercial aluminum alloy. This is done for the as-synthesized AAO layers, after various degrees of pore widening by a wet chemical etching in phosphoric acid solution, and upon surface modification by either Lauric acid or a silane. The as-grown AAO films feature structurally disordered pore architectures with average pore openings in the range 140−190 nm but with similar interpore distances of about 405 nm. The formation of such AAO structures induces a transition from slightly hydrophilic to moderately hydrophobic surfaces up to film thicknesses of about 6 μm. Increased hydrophobicity is obtained by pore opening and a maximum value of the water contact angle (WCA) of about 128° is measured for AAO arrays with a surface porosity close to 60%. Higher surface porosity by prolonged wet chemical etching leads to a rapid decrease in the WCA as a result of the limited pore wall thickness and partial collapse of the dead-end pore structures. Modification of the AAO surfaces by Lauric acid results in 5−30° higher WCA's, whereas near-superhydrophobicity (WCA ∼146°) is realized through silane coating. The "rose petal effect" of strongly hydrophobic wetting with high adhesive force on the produced AAO surfaces is explained by a partial penetration of water through capillary action into the dead-end pore cavities which leads to a wetting state in-between the Wenzel and Cassie states. Moreover, practical guidelines for the synthesis of rough, highly porous AAO structures with controlled wettability are provided and the possibility of forming superhydrophobic surfaces is evaluated.

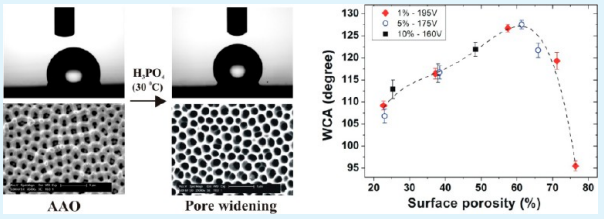

KEYWORDS: *anodic aluminum oxide (AAO), wettability, macropores, hard anodization, wet chemical etching, surface modification*

1. INTRODUCTION

Aluminum and its alloys are important industrial materials because of their low weight and good corrosion resistance thanks to surface passivation. One of the distinctive properties of aluminum is that when anodized under appropriate conditions, a porous structure can be formed on the surface.[1] Porous anodized aluminum oxide (AAO) membranes formed by the electrochemical anodization of aluminum have become a popular, low cost, and highly versatile material for applications in a wide range of fields such as surface tribology,[2] filtration,[3,4] catalysis,[5] biosensing,[6,7] and template synthesis of one-dimensional nanostructures.[8−11] The improved surface hardness and high porosity along with good thermal stability and chemical resistance are appealing assets of these inorganic porous membranes. Carefully controlled anodization of aluminum produces a thin (barrier) layer of dense aluminum oxide, followed by a self-organized hexagonal array of parallel pores aligned normal to the film surface. Self-ordered AAO arrays with well-controlled pore diameter (10−450 nm) and interpore distance (25−500 nm) are obtained by careful selection of the processing conditions, i.e., type and concentration of the acid electrolyte, applied anodization potential, current density, anodizing time, and temperature.[12−16] In the anodization process, there is a balance between the electric-field-enhanced oxide dissolution at the electrolyte/oxide interface and the formation of oxide at the oxide/metal interface.[17] The growth mechanism by which the porous AAO structures develop has been debated frequently,[18−24] and numerous attempts have been made to derive analytical expressions establishing the relations of the pore geometry and the electric field in the oxide with the parameters of the anodization process.[17]

Conventionally, AAO is fabricated under a so-called "mild anodization" (MA) conducted at low temperatures and employing sulfuric, oxalic, or phosphoric acid electrolytes. The self-ordering phenomenon of well-ordered, porous AAO occurs only in narrow process windows, known as self-ordering regimes.[12,15,25] In typical MA processes, the anodization working ranges and the resulting interpore distances are 10−25 V and 35−70 nm for sulfuric acid, 30−60 V and 80−150 nm for oxalic acid, and 160−195 V and 350−500 nm for phosphoric acid, respectively. However, under these MA conditions, the rate of oxide growth can be very low because of the low current density and the fabrication of self-ordered Al_2O_3 pore arrays might require several days of processing time.

Received: January 19, 2013
Accepted: March 18, 2013
Published: March 18, 2013

Therefore, the so-called "hard anodization" (HA) approach, which was invented in the 1960s[26] and involves much higher current densities, has been used in industry more widely for a high-speed fabrication of mechanically robust, very thick (>100 μm) and low-porosity alumina films. HA processes offer substantial advantages over conventional MA methods in terms of processing time and improved ordering of the nanopores.[16,25] A two-step anodizing procedure[11,17] is commonly used for the formation of high-ordered, porous AAO. Following an initial anodizing at the preselected potential, a wet chemical etching of the grown aluminum oxide layer is done. This oxide removal results in the generation of a periodic concave pattern on the aluminum surface, which acts as a template for the second anodizing step that is completed at the same anodizing potential as used for the first anodization.[11,17]

In recent years, the production of surfaces with special wettability, including superhydrophobicity, has attracted great research interest because of the promising potential for their use as self-cleaning surfaces and in microfluidics and droplet-based technologies.[27] By convention, a surface is called superhydrophobic when the effective contact angle (CA) of a liquid water droplet with the surface exceeds 150° and, on the other hand, superhydrophilic when the CA is smaller than 10°.[28] The issue of the large water contact angle (WCA) on plant leaves and animal surfaces was already addressed over 80 years ago by Wenzel, Cassie and Baxter, but only since the late 1990s, with the advances in wetting research and nanofabrication tools, the possibility to reach nearly perfect nonwettability on synthetic materials became reality.[29−32] In particular, for the synthesis of superhydrophobic materials a surface coverage with a low surface energy material is usually combined with a surface structuring with hierarchical topography at the nanometer and/or micrometer scale.

Due to the controllable pore dimension and adjustable surface chemistry, the porous AAO structures provide a great potential for producing surfaces with special wettability. Aluminum oxide itself has a certain tendency to be wetted by water and is therefore a hydrophilic material. The Young's CA of an intrinsic, smooth alumina surface is about 80°. However, combined with specific surface structure and/or surface chemistry, superhydrophobicity and also superhydrophilicity have recently been achieved on AAO surfaces.[33−37] Yao et al.[38] reported superhydrophobic, fractal alumina surfaces without any chemical modification in a study of diverse alumina architectures formed under high-field anodization in 0.3 M oxalic acid electrolytes. Ran and co-workers[39] indicated that the wettability of porous AAO changes from hydrophilicity to hydrophobicity by increasing the pore diameter while maintaining the interpore distance and pore depth constant. However, their investigation was based on just one pore architecture with average pore diameter and interpore distance of 260 and 400 nm, respectively. Superhydrophilic AAO films displaying a strongly disordered structure were produced by Ye et al. in a single-step, galvanostatic anodization in 0.3 M phosphoric acid electrolyte.[34] Alternatively, superhydrophobic surfaces were fabricated by either modifying the AAO surface using low surface energy materials or using AAO as a template for polymer synthesis. For instance, Mateo et al. showed that AAO films with pore sizes in the range 10−80 nm can be transformed from being superhydrophilic to superhydrophobic by coating the surface with a thin (2−3 nm) layer of a hydrophobic fluoropolymer.[37] In other works, various AAO structures were used as templates to replicate polytetrafluoroethylene polymeric materials displaying superhydrophobicity[40,41] and to obtain well-ordered polymer nanostructures[42] and biodegradable nanorod arrays[43] as well as polymer nanostructures with a wettability transition from wetting to nonwetting.[44] Surface modifications of anodized aluminum by silanes also proved successful in the formation of (super)-hydrophobic aluminum surfaces.[36,45,46]

Surface wettability of AAO structures has merely been studied in recent years. Yet, the number of literature reports on the wetting of AAO surfaces is limited and most of the studies were focused on their surface modification with low surface energy materials rather than systematically addressing the wetting of the inherently porous AAO architectures. This paper aims to provide further insight in the correlation between the structural characteristics and the surface wettability of macroporous AAO structures with pore sizes larger than 100 nm. The roughness-induced wettability is investigated systematically by varying the thickness and the porosity of oxide films grown by a two-step, high-field anodization in phosphoric acid of three different concentrations, independently. This is done for the as-synthesized AAO layers, after various degrees of pore opening by a wet chemical etching, and upon surface modification by Lauric acid or a silane using a commercial aluminum alloy. This study provides practical guidelines for the design of rough, highly porous AAO structures with controlled wettability and evaluates the possibility of forming superhydrophobic and highly porous aluminum oxide surfaces.

2. EXPERIMENTAL SECTION

2.1. Materials. A commercial aluminum alloy 1050 foil (min. 99.5% Al, max. 0.40% Fe, 0.15% Si, 0.03% Cu, 0.03% Mg, 0.03% Mn, Agfa-Gevaert, Belgium) with a thickness of 0.28 mm was used as the starting material for the preparation of AAO surfaces. Phosphoric acid (85%, Chem-Lab NV, Belgium), perchloric acid (70%, Acros Organics, Belgium), chromic oxide (99.99%, Vel NV, Belgium), acetone (>99%, Chem-Lab, Belgium), ethanol (99.9%, VWR International BVBA, Belgium), lauric acid (>98%, Sigma-Aldrich, Belgium), and 1H,1H,2H,2H perfluorodecyltrichlorosilane (97%, abcr GmbH & Co. KG, Germany) were used as-received.

2.2. Preparation of AAO Surfaces. The aluminum alloy foil was cut into 25 × 15 mm^2 pieces and, as a cleaning step prior to the anodization process, all the samples were first degreased with acetone and then rinsed with deionized water. Both steps were carried out in an ultrasonic bath (Branson 1510). Subsequently, electropolishing was done at 10 °C for 1 min in a mixture of perchloric acid and ethanol (1:4, v/v). The mirror polished aluminum pieces were placed in a two-electrode cell with a parallel electrode arrangement using a Pt mesh as cathode. A two-step hard anodization process was performed in potentiostatic mode using a medium voltage power supply (MCL 350−650) applying constant anodization voltages of 160, 175, and 195 V in electrolytes of 10, 5, and 1 wt % phosphoric acid, respectively, keeping the temperature in the cell at 0 °C. After 60 min of first anodization, the alumina layer was removed from the aluminum substrate using a mixture of 6 wt % phosphoric acid and 1.8 wt % chromic oxide in deionized water at 60 °C, leaving a highly ordered concave pattern on the surface of the samples (see Figure S1 in the Supporting Information). Following, a second anodizing step was carried out on the surface-patterned aluminum, resulting in macroporous alumina arrays of increased regularity. The second anodizing step was performed for anodization times varying from 15 to 300 min in order to produce AAO layers with increasing film thickness. A wet chemical etching (or postetching) in 5 wt % phosphoric acid at 30 °C was applied to a selection of AAO samples for pore widening, while keeping the interpore distance constant. Hereto, etching times of 60, 100, 120, and 150 min were selected. After both the two-step HA and wet chemical etching processes, all the samples were ultrasonically

cleaned with acetone for 10 min and then rinsed with deionized water. They were placed into a vacuum stove heated to 70 °C for 6 h to completely dry the porous surface structures.

2.3. Modification of AAO Surfaces. Modification of a selection of AAO surfaces was done using two different surfactants, i.e. Lauric acid ($C_{12}H_{24}O_2$, CAS: 143−07−7) and 1H,1H,2H,2H perfluorodecyltrichlorosilane (CAS: 78560−44−8). Samples were immersed into 5 wt % Lauric acid solution for 90 min and dried in air for one day. Alternatively, an oven was prebaked at 140 °C for 30 min and, then, 10 μL of the corresponding silane was placed on a glass substrate about 4 cm distant from the sample positioned toward the outlet of the gases. The whole system was brought to vacuum and kept at 140 °C during another 30 min.

2.4. Characterization. Top view and cross-sectional structural characterization of the prepared AAO surfaces was done using a field emission scanning electron microscope (SEM; Philips XL 30 FEG) operated in secondary electron mode. Samples were mounted on a holder with double sided conductive carbon tape and sputter coated (Type BU-07120, Balzers Union, Liechtenstein) with a thin layer of gold. During this coating process, the samples were positioned on a stage 5 cm below the Au target and the deposition current and time were set at 20 mA and 20 s, respectively. SEM and ImageJ (Version 1.46) software were used to analyze independently the average pore size, interpore distance, pore wall thickness, and surface porosity (defined as the fraction of surface area made up by pores to the whole surface area) of the prepared AAO layers. Static (sessile drop) WCA's were determined on the AAO surfaces using a Kruess drop shape analysis system (DSA 10-Mk2, Kruess, Germany) applying water droplets of about 1 μL. Fourier transform infrared (FTIR) spectroscopy (Thermo Optek, Avatar 370) was used to study the surface chemistry of the modified samples.

3. RESULTS AND DISCUSSION

Analysis of the surface morphologies of AAO films formed after the two-step anodization in the three different electrolytes reveals a strong resemblance between the produced pore structures. Figure 1 shows typical SEM images of the surfaces of about 2.5 μm thick AAO layers grown from the 1, 5, and 10 wt % phosphoric acid electrolytes, respectively. In all three cases, porous oxide layers are formed with relatively broad distributions of surface pore openings. With increasing electrolyte concentration, the AAO structures feature slightly increasing average values of the pore openings of about 140, 150, and 190 nm, respectively. The AAO surfaces display similar interpore distances of about 405 nm, but the pores are not perfectly ordered. In fact, disordered pore architectures are developed, because the nearest neighbor is not necessarily arranged hexagonally as determined by the radial distribution function. Note that a significant fraction of the pore channels is interconnected as they are exposed to the surface in larger single pore openings (Figure 1).

Apart from anodization potential and pH of the electrolyte solution, the porosity of the AAO nanostructures formed in phosphoric acid solutions may also be affected by the anodizing time, an extension of which usually results in increasing porosity.[17,47] Here, we have studied the pore arrangement, the growth rate, and the surface porosity as a function of anodizing time (or AAO layer thickness) in the 1 wt % phosphoric acid electrolyte. Figure 2 shows the cross-sectional SEM images of a selection of AAO films produced with anodizing times varying from 15 up to 300 min. The development of a porous AAO layer characterized by aligned pores is evident. A nearly constant thickness of the barrier oxide layer of about 150 nm is observed throughout. The surface porosity was found to be nearly constant (about 20−25%) as well, but the pore arrangement in the AAO layer is somewhat disorganized. The

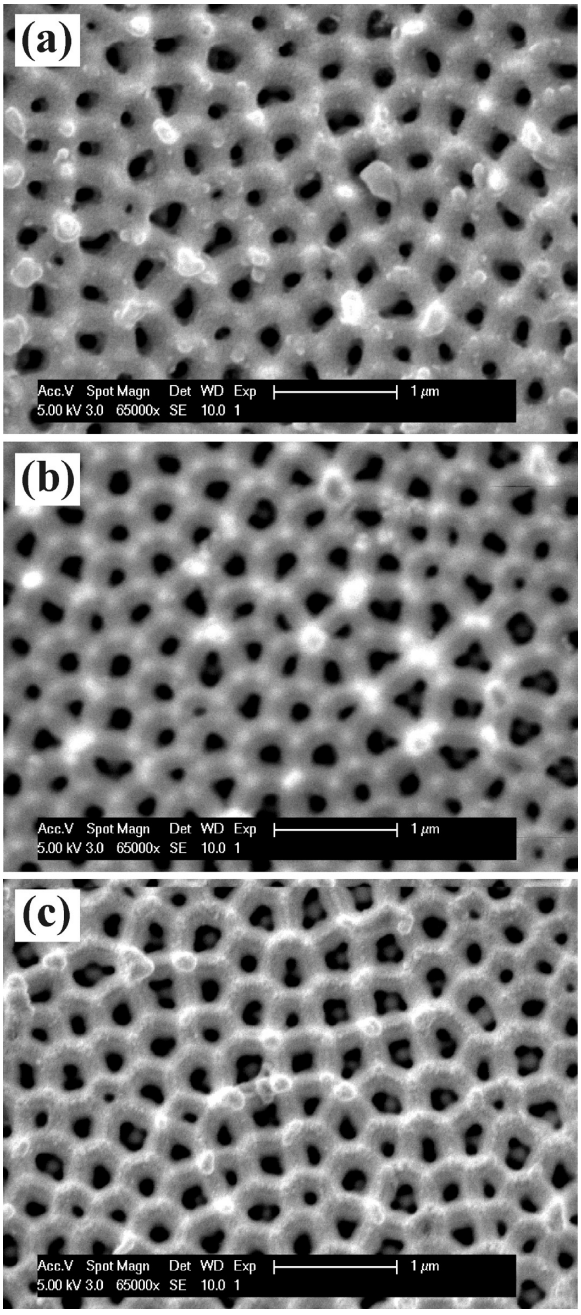

Figure 1. Top-view SEM images of 2.5 μm thick AAO layers formed after two-step hard anodizing in three different phosphoric acid electrolytes with varying anodization potentials: (a) 1 wt % at 195 V, (b) 5 wt % at 175 V, and (c) 10 wt % at 160 V.

distribution of pore diameters is quite broad and there is a lack of uniformity along the pore axis. After 300 min of anodizing, the AAO layer thickness is about 7.9 μm which corresponds to a value of the aspect ratio close to 50. The thickness of the AAO film as a function of the duration of the second anodization step is displayed in Figure 3. A practically linear dependence with an average growth rate of about 1.7 μm h^{-1} (coefficient of determination R^2 is 0.985) is derived. This value is significantly lower than expected for our HA conditions, although the steady-state current density (see Figure S2 in the Supporting Information) applied was not extraordinarily high, i.e., in the range of about 4−8 mA/cm^2 for this particular anodization condition. In other studies on HA in phosphoric

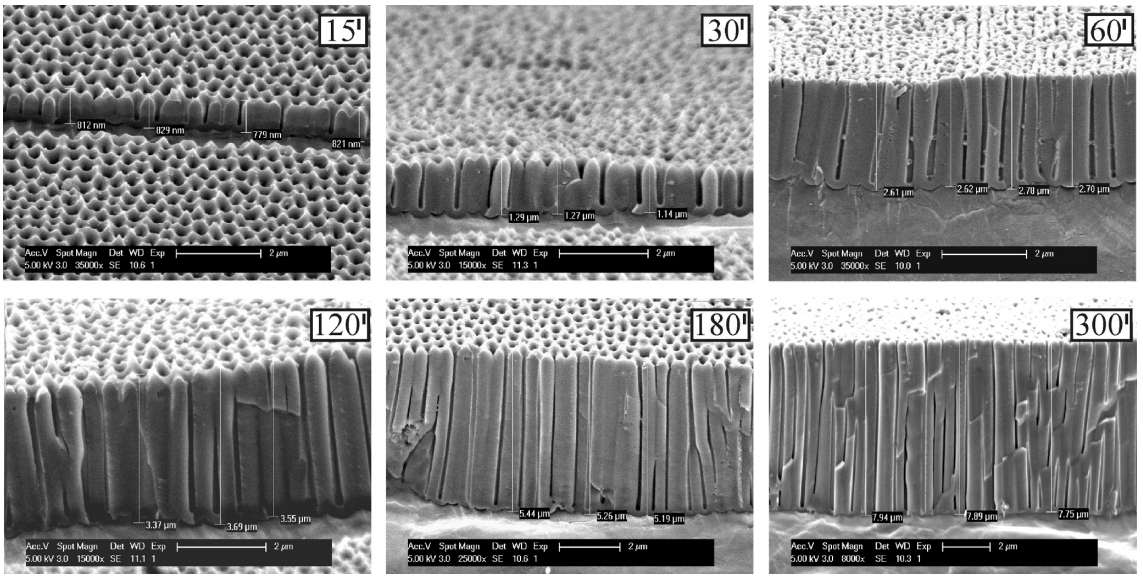

Figure 2. Cross-sectional SEM images of a selection of AAO films produced with anodizing times varying from 15 up to 300 min in 1 wt % phosphoric acid (anodization voltage of 195 V).

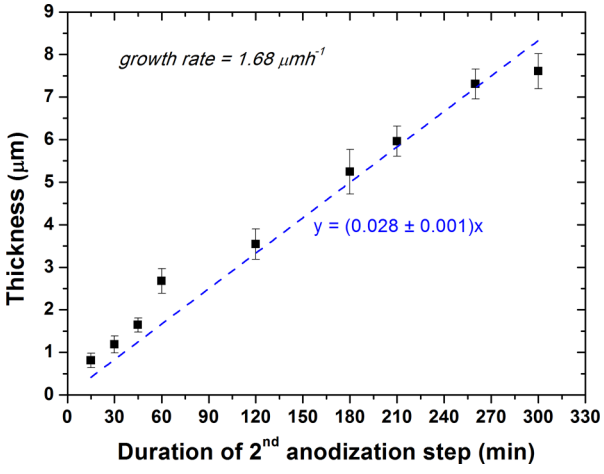

Figure 3. Thickness of the AAO layer as a function of the duration of the second anodization step for anodizing in 1 wt % phosphoric acid electrolyte at 195 V. The dashed line shows the linear best fit through the data points.

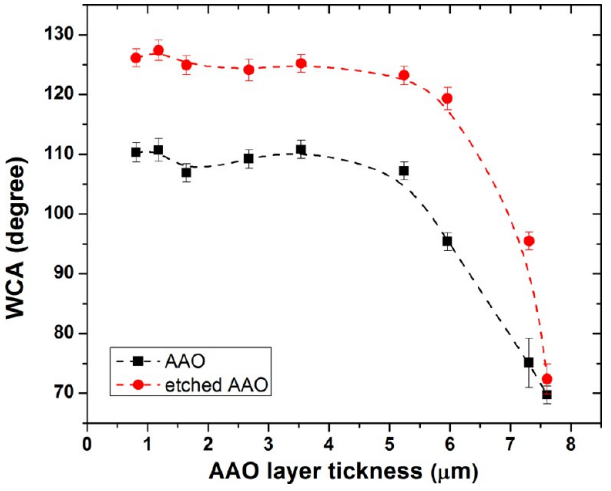

Figure 4. Water contact angle (WCA) as a function of the layer thickness of AAO produced in 1 wt % phosphoric acid (anodization voltage of 195 V). The square symbols refer to as-synthesized AAO and the round symbols denote the values after a wet chemical etching in 5 wt % phosphoric acid at 30 °C.

acid, much higher current densities (up to 70 mA/cm^2) have been employed.[48]

The water contact angle (WCA) as a function of the AAO layer thickness is plotted in Figure 4 (lower curve). Clearly, the produced porous AAO structures give rise to moderately hydrophobic surfaces (WCA >90°) up to layer thicknesses of about 6 μm. The WCA is more or less constant at 110° for an oxide thickness up to 5 μm, whereas for thicker AAO layers the WCA drops drastically and reaches a value of about 70° for 7.5 μm thick layers. To investigate the effect of a pore opening on the wetting of these AAO surfaces, we etched the AAO surfaces in 5 wt % phosphoric acid at 30 °C. The pore widening results in a shift of the WCA toward higher values by about 15° (i.e., the surfaces become more hydrophobic) for an AAO layer thickness up to 5 μm (Figure 4, upper curve). Eventually, the WCA drops to a value similar to that of the as-grown oxide structure when the layer thickness is about 7.5 μm. Structural characterization showed that the pore widening results in a strong increase in the surface porosity from about 25 to 65% without affecting the pore density and AAO layer thickness.

To study the effect of the pore opening on the wetting of AAO in more detail, we varied the etching time and the resulting oxide structures were characterized systematically. Top view and cross-sectional SEM images of a series of wet chemical etched AAO structures after different etching times are shown in Figure 5. The progressive pore widening with etching time is evident. The pore wall thickness decreases and consequently both the average pore diameter and the surface porosity increase. Figure 6a shows the pore size distribution of the initial AAO layer formed after 30 min of anodizing in 5 wt % phosphoric acid (anodizing voltage of 175 V). A near Gaussian distribution around an average value of 141 ± 42 nm is derived for this as-grown AAO structure. After 120 min of wet chemical etching (Figure 5d), the pore size distribution (Figure 6b) has changed drastically and an average pore

dx.doi.org/10.1021/am4001425 | ACS Appl. Mater. Interfaces 2013, 5, 3224−3233

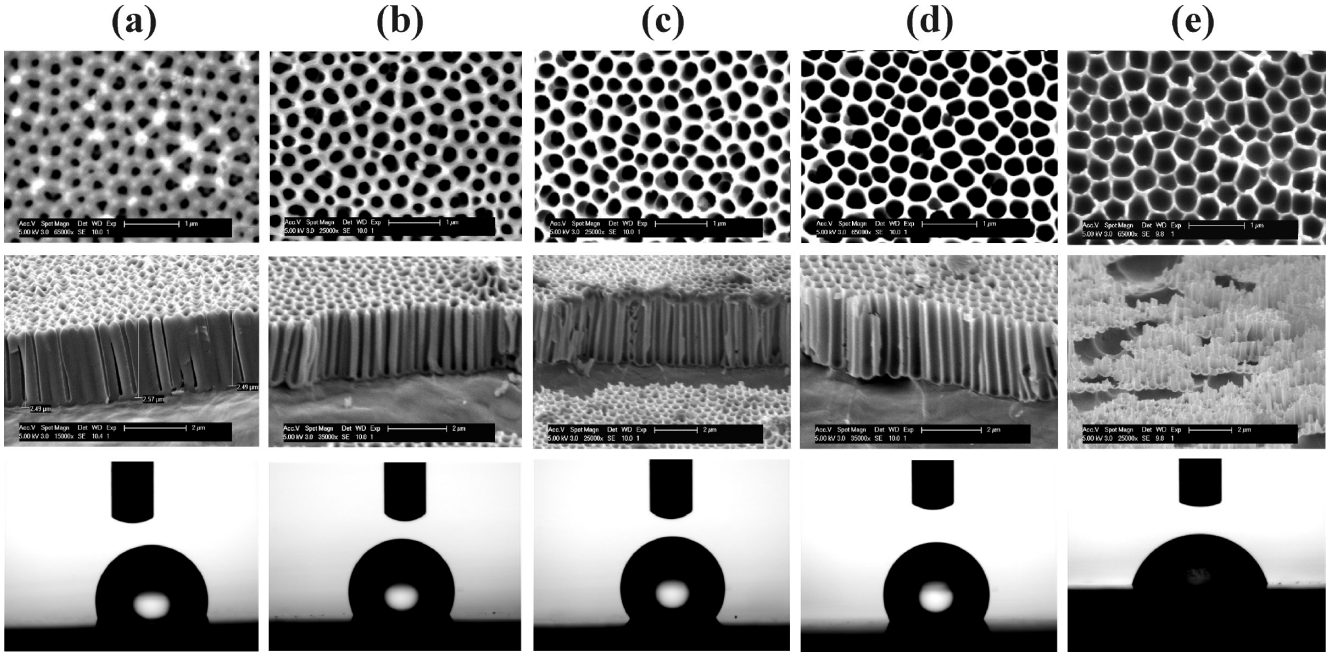

Figure 5. SEM images in top view (upper row) and cross-sectional view (middle row) of and 1 μL water droplets (lower row) on AAO formed after 30 min of anodizing in 5 wt % phosphoric acid (anodization voltage of 175 V) followed by a pore widening using different etching times: (a) 0, (b) 60, (c) 100, (d) 120, and (e) 150 min. Wet chemical etching in 5 wt % phosphoric acid at 30 °C was done for the pore widening.

diameter of 331 ± 42 nm is obtained. The average values of the pore size, interpore distance, pore wall thickness, and surface porosity as a function of the etching time are summarized in Table 1. For example, after 60 min of etching, the pore size and surface porosity increase by a factor of about 1.6 and after 150 min the pore size is even 2.5 times larger than that of the as-grown AAO structure. Importantly, there is a strong effect of the etching time on the pore size, pore wall thickness, and surface porosity, while the interpore distance (about 405 nm) remains unaffected.

Measurement of the WCA (Figure 5, lower row) reveals a maximum value of 127.5° ± 1.0° after 100 min of wet chemical etching (Figure 5c and Table 1). After 120 min of etching, the WCA decreases slightly to 121.7° ± 1.6°. However, after 150 min of etching, the WCA drops radically by another 46° down to 75.7° ± 1.8°, which corresponds to a hydrophilic surface. This abrupt change in wetting is likely caused by an overetching of the porous AAO structure. SEM analysis of the AAO layer after 150 min of wet chemical etching reveals a limited pore wall thickness of only 43 ± 18 nm and also a collapse of the dead-end pore structure in certain areas of the sample surface (Figure 5e, middle row).

Overall, the wetting of the AAO surfaces is largely dependent on the surface porosity. The WCA as a function of the surface porosity for different as-grown and etched AAO structures is plotted in Figure 7. Surface porosity in the range from 20 to 25% corresponds to as-prepared AAO, whereas the range from 37 to 77% is covered by etched AAO samples. The WCA follows a nearly linear relationship with the surface porosity in the range from 20 to 60%; the higher the fraction of free surface, the larger the WCA. This trend of increasing hydrophobicity of the AAO surface with porosity seems to be independent of the anodization conditions, which supports our previous finding that it is possible to produce AAO topographies with similar pore characteristics under hard anodizing in phosphoric acid with different combinations of the electrolyte concentration and anodization voltage, and etching time. However, the WCA drops quickly for values of the surface porosity larger than 60%. Likely, with increasing etching time or pore opening, the pore walls become too thin to either maintain the two-dimensionally aligned porous AAO structure (i.e., film breakdown occurs) or to support the water droplet and, as a result, water spreads easily, thereby decreasing the hydrophobicity of the surface.

The controllable porosity of the AAO surfaces combined with an adjustable surface chemistry provides a large potential for producing surfaces with enhanced hydrophobicity. Figure 8 displays the values of the WCA on the surface of the pristine, nonporous aluminum foil and on a series of etched AAO surfaces, before and after a surface modification by Lauric acid, respectively. The untreated aluminum foil (filled diamond symbol) displays a WCA of 80.6° ± 1.9°, which is comparable to the value of 85 ± 3° measured on a solid alumina surface[39] and can thus be explained by the presence of a native oxide surface layer.[49] An enlargement of the WCA by about 9° is obtained with a surface modification using Lauric acid (open diamond symbol). A similar trend is observed for the AAO surfaces. The surface modification with Lauric acid results in values of the WCA enlarged by 5° up to 30° (open rectangular symbols) but the overall trend of the WCA as a function of the etching time is still maintained. The highest WCA (135.6 ± 1.0°) is obtained for the AAO surface being etched for 100 min followed by a surface modification with Lauric acid, being about 8° higher than that measured on the etched AAO surface without Lauric acid.

A direct comparison between the WCA's measured on a selection of untreated and surface modified aluminum and AAO surfaces is given in Figure 9. The surface of the as-received aluminum foil (Figure 9a) is slightly hydrophilic (WCA about 81°). As discussed above, a surface modification using Lauric acid leads to an increased hydrophobicity (Figure 9b). The formation of a porous AAO structure results in further

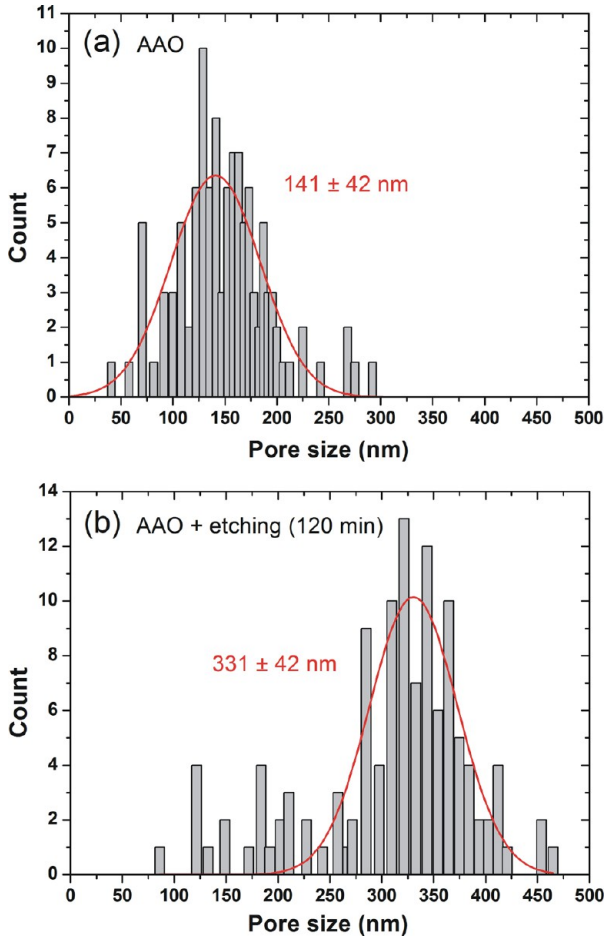

Figure 6. Pore size distribution diagrams of (a) AAO formed after 30 min of anodizing in 5 wt % phosphoric acid (anodization voltage of 175 V) and (b) after a subsequent pore widening by a wet chemical etching in 5 wt % phosphoric acid at 30 °C for 120 min. The solid red lines represent the Gaussian best fits through the experimental data.

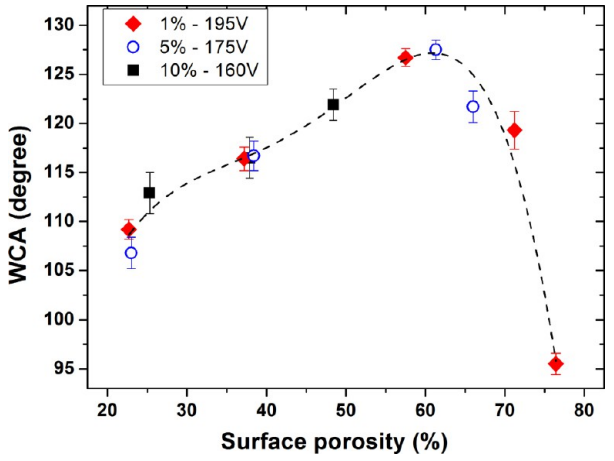

Figure 7. WCA as a function of the surface porosity for AAO formed after different anodizing and etching treatments. Diamond, circle, and square symbols represent data for anodizing in 1, 5, and 10 wt % phosphoric acid electrolyte, respectively.

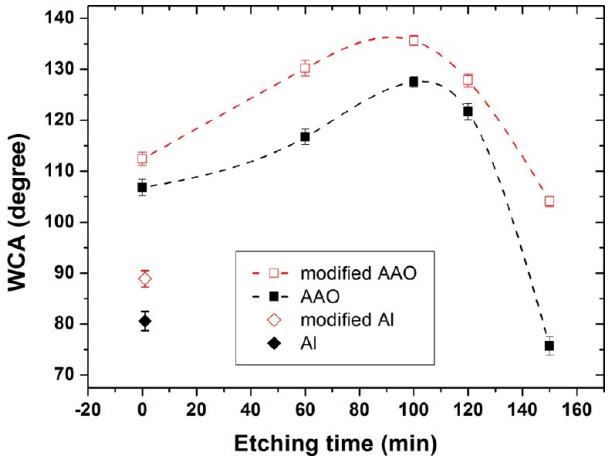

Figure 8. WCA for the as-received aluminum foil (filled diamond symbol) and the aluminum foil modified with Lauric acid (open diamond symbol) and WCA as a function of etching time for AAO without (filled square symbols) and with (open square symbols) a surface modification by Lauric acid. The AAO was produced by anodizing for 30 min in 5 wt % phosphoric acid (anodization voltage of 175 V). Wet chemical etching was done in 5 wt % phosphoric acid at 30 °C. Surface modification was done by immersion into 5 wt % Lauric acid solution for 90 min.

enhanced hydrophobicity (Figure 9c) and that effect is strengthened by an additional pore opening (Figure 9d). When a silane is used for the surface modification of a strongly hydrophobic AAO surface with a WCA of about 127°, which was formed after hard anodizing in 1 wt % phosphoric acid followed by a wet chemical etching for 150 min (Figure 9e), near-superhydrophobicity is reached (Figure 9f). The corresponding WCA of 146° is only slightly less than the necessary 150° for a truly superhydrophobic surface, which shows that the combination of a highly porous AAO surface and an optimized chemical modification with silanes is most promising for the production of superhydrophobic aluminum oxide surfaces.

The AAO structures formed after the two-step hard anodization of the aluminum alloy (Figure 1) are not perfectly ordered as is the case for anodization of highly pure (typically >99.99%) aluminum in the self-ordering regime in phosphoric acid.[17] In this respect, a detrimental effect of the higher

Table 1. Average Values of the Pore Size, Inter-Pore Distance, Pore Wall Thickness, Surface Porosity, And Water Contact Angle (WCA) as a Function of the Etching Time for AAO Formed after 30 min of Anodizing in 5 wt % Phosphoric Acid (anodization voltage of 175 V)

etching time (min)	pore size (nm)	interpore distance (nm)	pore wall thickness (nm)	surface porosity (%)	WCA (deg)
0	141 ± 42	403 ± 55	264 ± 39	23	106.8 ± 1.6
60	220 ± 40	396 ± 61	188 ± 35	38	116.7 ± 1.5
100	297 ± 43	414 ± 56	115 ± 26	61	127.5 ± 1.0
120	331 ± 42	402 ± 61	68 ± 15	66	121.7 ± 1.6
150	354 ± 48	415 ± 53	43 ± 18	73	75.7 ± 1.8

dx.doi.org/10.1021/am4001425 | ACS Appl. Mater. Interfaces 2013, 5, 3224−3233

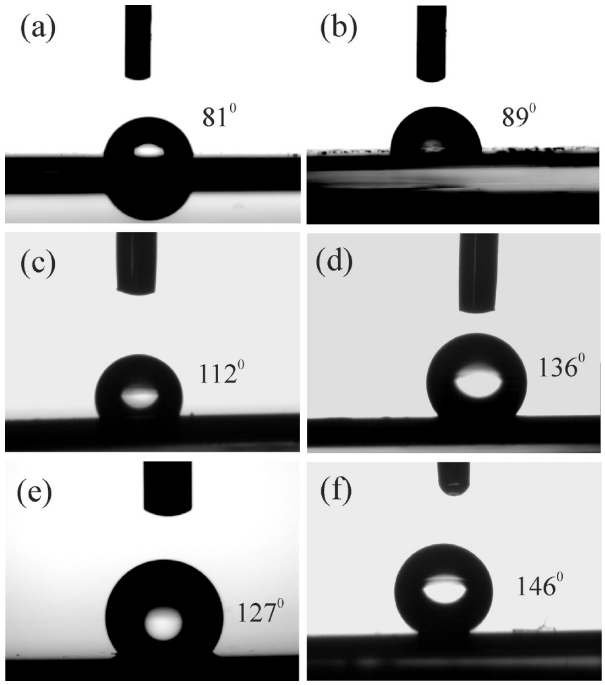

Figure 9. WCA measurements on a selection of untreated and surface modified aluminum and AAO surfaces: (a) as-received aluminum foil, (b) aluminum foil after modification with Lauric acid, (c) AAO formed by anodizing in 5 wt % phosphoric acid after modification with Lauric acid, (d) AAO formed by anodizing in 5 wt % phosphoric acid, followed by 100 min of wet chemical etching and modification with Lauric acid, (e) AAO formed by anodizing in 1 wt % phosphoric acid and 100 min of wet chemical etching, and (f) AAO formed by anodizing in 1 wt % phosphoric acid, followed by 100 min of wet chemical etching and modification with a silane.

concentrations of alloying elements such as Fe and Si in the 1050 aluminum alloy (>99.5%) on the ordering of pores in our AAO structures is expected.[11] Nielsch et al.[50] reported that, for a perfect hexagonal arrangement of nanopores formed by self-organized anodization under optimum anodizing conditions, the ratio between pore diameter and interpore distance is equal to about 0.33, fulfilling a 10% porosity rule.[17] However, there is a limited number of and a great inconsistency among experimental data on the porosity of AAO nanostructures formed in phosphoric acid electrolytes. In the disordered growth regime, the porosity can be significantly larger or even smaller than 10%.[51,52] For example, the porosity is about 40% using 160 V instead of 195 V in 0.1 M H_3PO_4.[50] The oxide films synthesized in this work display values of the surface porosity in the range 20−25%.

Our results show an increase in the hydrophobicity of macroporous AAO with the average pore diameter, which can be controlled by an etching step (up to the limit of pore collapse). Thus, larger interpore distances would allow to eventually achieve larger pore sizes after an etching step. Hydrophobicity could also be increased by delaying pore collapse by fabricating layers with well-organized pores. Because MA often results in larger interpore distances and improved pore ordering as compared to HA, MA growth processes may have some merits to the HA conditions applied in this study.

The increased surface roughness of the AAO surfaces effectively enlarges the liquid−solid free energy. Strong water repellence is the consequence of either a larger effective contact area between the two components, the case of the liquid impregnating the surface (the so-called Wenzel state), or a replacement of the true liquid−solid contact by a highly energetic liquid−vapor interface.[32] The latter is the case when the liquid interface is suspended on an air cushion enclosed by roughness peaks (the so-called Cassie or fakir state). The Wenzel's and Cassie−Baxter models alone cannot be used to explain the wettability performance of the porous AAO structures. A coexisting model[53] describing a state in-between the Wenzel and Cassie states might be more appropriate to explain the wetting in the case of a water droplet placed on the AAO surfaces. Water will likely penetrate into the pores with a certain depth, but not completely. In this way, air is sealed in the dead-end pore cavities, forming a kind of "air pockets" and a composite interface is formed, which consists of both solid−liquid and liquid−air fractional interfaces. To predict the penetration of a water droplet into each of the pores, a pressure balance model can be used,[37,39] which is based on the assumption that when water wets the porous alumina surface, the air in the pore is not expelled but compressed. At the liquid−air interface, a force balance exists between the force exerted by the compressed air and the sum of the capillary force and the gravity force (i.e., the weight of the water column above the air pocket). The capillary force, F_c, can be expressed as

$$F_c = \pi\gamma d \cos\theta \quad (1)$$

where γ, d, and θ are the surface tension of water, pore diameter, and Young's CA, respectively.[54] The gravity force is relatively small compared to the capillary force, so the capillary force is balanced by the air resistance. If it is assumed that the air trapped inside the pores behaves like an ideal gas obeying Boyle's law and if the size of the pores is much smaller than the size of the water droplet, the displacement of water into the pore, h, can be expressed as

$$h = 4L\gamma \cos\theta/(P_0 d + 4\gamma\cos\theta) \quad (2)$$

where L and P_0 are the pore depth and atmospheric pressure, respectively.[39,55]

From the above analysis, the presence of a coexisting state for the wetting of AAO surfaces becomes clear. In the case of the as-grown AAO layers, the pore diameter is about 140 nm. Using the values of the Young's CA for an intrinsic, smooth alumina surface $\theta \approx 80°$ and $\gamma = 72$ mN/m in eq 2, one obtains $h/L \approx 0.77$. This means that about 77% of the porous volume or pore depth is filled with water and the wetting is a near-Wenzel intermediate state. On the other hand, after 120 min of wet chemical etching, the pore diameter increases to about 330 nm. This results in a reduced water penetration to about 60%, indicating a situation more close to the Cassie state. The wettability of the as-prepared and etched AAO surfaces does not effectively change within a certain range of oxide layer thickness (Figure 4). The nearly constant values of the WCA of 110 and 125° for the as-prepared and etched AAO surfaces, respectively, before reaching a critical value of the film thickness close to 5 μm can be understood from the above model of an intermediate wetting state. However, it does not explain the sudden change of the WCA at this certain critical thickness. Above this thickness value, which is probably also determined by the pore size (diameter), the surface becomes hydrophilic. The exact reason for this drop in WCA remains unclear, but it could be the result of an ineffective removal of electrolyte after sample preparation, becoming progressively complicated with increasing pore depth (i.e., film thickness). Experimental evidence of remaining phosphorus contamination as a result

of the incorporation of phosphate anions in the oxide layer due to the electric field during anodization, even after sample cleaning, was derived from energy dispersive X-ray analysis of our samples (not shown). However, differences in the amount of phosphorus content with pore depth need to be confirmed.

According to eq 2, the penetration depth of water is proportional to the depth of the dead-end pores, but the extent of water infiltration decreases with increasing pore size (diameter). Thus, with increasing pore size, a shift toward a wetting closer to the Cassie state is foreseen. This fits with the observed increase in WCA up to 100 min of etching (Figure 5 and Table 1). For longer etching times, values of the WCA drop drastically and likely the more desirable Cassie-like state is destabilized in favor of a more Wenzel-like state. This Cassie-to-Wenzel transition involves the impregnation of the roughness features of the AAO surface with water, and it can occur for a number of reasons, such as the presence of surface defects.[32] The observed limited pore wall thickness and partial collapse of the dead-end pore structure after prolonged etching (Figure 5d, e) could account for a mechanically weak and three-dimensionally porous, capillary surface structure into which the water droplet would spread more easily. This is supported by a small reduction in size of the water droplets placed on top of these overetched sample surfaces over time (several minutes) as observed during the WCA measurements. As a result of wicking and imbibition effects,[56] which are dependent on the surface roughness and solid fraction, the water drop lays on a composite solid/liquid surface which could lead to a large reduction of the WCA. In this respect, Ye et al.[34] also demonstrated that a reduction of the air-pocket effect in mixed 2D/3D capillary structures of single-anodized alumina leads to a strongly enhanced hydrophilicity.

An attractive aspect of the wetting of the AAO structures with pore sizes up to about 330 nm is the 'sticky' hydrophobicity. The water droplets are highly adhesive and we observed that they are held in place against gravity even when the surface is flipped upside down (see Figure S3 in the Supporting Information). This is a result of the ingress of water into the pores by the capillary action and the large surface tension of water.[37] It resembles the so-called "rose petal effect"[57] of very high WCA's coexisting with strong adhesion between the water and the solid surface. Similarly, a strongly hydrophobic state with high adhesive force was also observed for AAO films with pore diameters in the range 10−80 nm and coated with a thin layer of hydrophobic polymer.[37]

Chemical modification of the porous AAO structures provides a key solution for the production of strongly hydrophobic or even superhydrophobic surfaces. In this study, we have shown that a modification with either a silane by thermal evaporation or with Lauric acid via liquid immersion enhances the hydrophobicity of the produced AAO films. Best results were obtained with the silane, which is frequently applied for the production of antireflective and soil-repellent coatings. However, surface treatment with the low surface energy material Lauric acid is attractive as well, since Lauric acid is inexpensive, nontoxic and safe to handle. The bonding of Lauric acid on the AAO surfaces is a kind of self-assembly process. It was found that the WCA increases almost linearly with modification time until around 90 min, after which it remains constant (see Figure S4 in the Supporting Information). This saturation is likely the result of reaching a full surface coverage by Lauric acid. For too short immersion times, the sluggish diffusion kinetics limit the formation of such a complete, thermodynamically controlled monolayer. FTIR spectra taken from the modified AAO surfaces appeared strikingly similar to that of the pure Lauric acid powder, which proves a successful assembly of Lauric acid molecules onto the AAO surfaces. The stability of this modification was investigated by measuring the WCA on the same sample with intervals of several days. It was found that the WCA was nearly unchanged after 15 days (i.e., a slight decrease by only about 2° was measured). This indicates that the bonding between the self-assembled monolayer and the AAO surface is quite stable. It is expected that the Lauric acid molecules use the carboxylic −COOH groups to bond to the alumina surface, leaving the long apolar alkyl chains on the outer surface. This results in a highly nonpolar surface chemistry that further increases the hydrophobicity of the AAO samples. However, it seems impossible to reach WCA's at the level of superhydrophobicity (i.e., >150°) like was recently reported by Ruan et al. for aluminum surfaces etched in a Beck's dislocation etchant (mixture of HCl and HF) followed by an immersion in a Lauric acid-ethanol solution.[58] Further experimental work is therefore needed to study the bonding of the Lauric acid molecules, for example, whether the interior pore walls are covered effectively as well. Nevertheless, optimization of the surface modification by silane coating seems most promising in achieving truly superhydrophobic porous aluminum oxide surfaces.

4. CONCLUSION

In conclusion, we have demonstrated a structure-induced transformation from slightly hydrophilic to moderately hydrophobic surfaces when highly porous anodic aluminum oxide is formed on the surface of an aluminum alloy. The correlation between the structural characteristics and the roughness-induced wettability of the AAO surfaces was investigated by varying the thickness and the porosity of the porous oxide films independently. Disordered pore architectures with average pore sizes in the range 140−190 nm but with similar interpore distances of about 405 nm were grown by a two-step, high-field anodization in phosphoric acid of three different concentrations. The as-grown AAO surfaces exhibit nearly constant WCA values of about 110° for film thicknesses up to about 5 μm. Enhanced hydrophobicity of these AAO structures is obtained with various degrees of pore opening by a wet chemical etching in phosphoric acid solution. A strong correlation between the water contact angle and the surface porosity is found and the highest value (i.e., WCA ∼128°) is measured for AAO arrays with a surface porosity close to 60%. Higher surface porosity by prolonged wet chemical etching leads to a rapid decrease in the WCA as a result of the limited pore wall thickness and partial collapse of the dead-end pore structures. The "rose petal effect" of strongly hydrophobic wetting with high adhesive force on the produced, highly porous AAO surfaces is explained by a partial penetration of water through capillary action into the dead-end pore cavities and a wetting state in-between the Wenzel and Cassie states. Finally, the possibility of forming superhydrophobic surfaces was evaluated for chemical modification of the AAO structures by either immersing into Lauric acid solution or by coating with a silane via thermal evaporation. Best results were obtained with the silane (WCA ∼146°), although the self-assembly process of the bonding of Lauric acid also holds a certain potential as an inexpensive and stable low surface energy material on highly porous AAO films.

■ ASSOCIATED CONTENT

Supporting Information

Top-view SEM images illustrating the topographical changes of the AAO surface after each of the main processing steps (i.e., after a first anodization, oxide removal, second anodization, and wet chemical etching), typical current density graphs recorded during the second anodization step for the three different electrolyte concentration−anodization voltage pairs (1 wt %−195 V, 5 wt %−175 V, 10 wt %−160 V), optical images showing 1 μL water droplets (WCA about 122°) on hydrophobic AAO surfaces prepared in 1 wt % phosphoric acid electrolyte at 195 V in both up- and downward positioning of the sample, and a graph of the WCA vs immersion time of the Lauric acid modification treatment for AAO prepared in 5 wt % phosphoric acid electrolyte at 175 V and 100 min of wet chemical etching for pore opening. This material is available free of charge via the Internet at http://pubs.acs.org.

■ AUTHOR INFORMATION

Corresponding Author

*E-mail: Ivan.Buijnsters@mtm.kuleuven.be. Phone: + +32 (0) 16 32 12 60. Fax: +32 (0)16 32 19 91.

Notes

The authors declare no competing financial interest.

■ ACKNOWLEDGMENTS

The authors acknowledge funding from the European Community's Seventh Framework Programme of Research for SME's (FP7-SME-2010) under Grant Agreement 262078 and of Marie Curie Actions IRSES projects TEMADEP (247659) and OIL&SUGAR (295202). Irene Kwee and Luis González-Urbina are acknowledged for their technical assistance. J.G.B. and N.T. thank the Executive Research Agency of the European Union for funding under the Marie Curie grants NANODIA (272448) and NANOALLOY (252407/909407).

■ REFERENCES

(1) Keller, F.; Hunter, M. S.; Robinson, D. L. *J. Electrochem. Soc.* **1953**, *100*, 411−419.

(2) Vojkuvka, L.; Santos, A.; Pallarès, J.; Ferré-Borrull, J.; Marsal, L. F.; Celis, J. P. *Surf. Coat. Technol.* **2012**, *206*, 2115−2124.

(3) Urase, T.; Yamamoto, K.; Ohgaki, S. *J. Membr. Sci.* **1996**, *115*, 21−29.

(4) Yang, S. Y.; Ryu, I.; Kim, H. Y.; Kim, J. K.; Jang, S. K.; Russell, T. P. *Adv. Mater.* **2006**, *18*, 709−712.

(5) Liu, F.; Lee, J. Y.; Zhou, W. J. *Small* **2006**, *2*, 121−128.

(6) ter Maat, J.; Regeling, R.; Ingham, C. J.; Weijers, C. A. G. M.; Giesbers, M.; de Vos, W. M.; Zuilhof, H. *Langmuir* **2011**, *27*, 13606−13617.

(7) Kumeria, T.; Losic, D. *Nanoscale Res. Lett.* **2012**, *7*, 88.

(8) Lee, J.; Kim, J.; Hyeon, T. *Adv. Mater.* **2006**, *18*, 2073−2094.

(9) Sarkar, J.; Khan, G. G.; Basumallick, A. *Bull. Mater. Sci.* **2007**, *30*, 271−290.

(10) Ciambelli, P.; Arurault, L.; Sarno, M.; Fontorbes, S.; Leone, C.; Datas, L.; Sannino, D.; Lenormand, P.; Le Blond Du Plouy, S. *Nanotechnology* **2011**, *22*, 265613.

(11) Martín, J.; Maiz, J.; Sacristan, J.; Mijangos, C. *Polymer* **2012**, *53*, 1149−1166.

(12) Masuda, H.; Fukuda, K. *Science* **1995**, *268*, 1466−1468.

(13) Masuda, H.; Satoh, M. *Jpn. J. Appl. Phys.* **1996**, *35*, L126−L129.

(14) Masuda, H.; Yada, K.; Osaka, A. *Jpn. J. Appl. Phys.* **1998**, *37*, L1340−L1342.

(15) Li, A. P.; Müller, F.; Birner, A.; Nielsch, K.; Gösele, U. *J. Appl. Phys.* **1998**, *84*, 6023−6026.

(16) Schwirn, K.; Lee, W.; Hillebrand, R.; Steinhart, M.; Nielsch, K.; Gösele, U. *ACS Nano* **2008**, *2*, 302−310.

(17) Sulka, G. D. Highly Ordered Anodic Porous Alumina Formation by Self-Organized Anodizing. In *Nanostructured Materials in Electrochemistry*; Eftekhari, A., Ed.; Wiley-VCH: Weinheim, Germany, 2008; pp 1−116.

(18) Hoar, T. P.; Mott, N. F. *J. Phys. Chem. Solids* **1959**, *9*, 97−99.

(19) O'Sullivan, J. P.; Wood, G. C. *Proc. R. Soc. London, Ser. A* **1970**, *317*, 511−543.

(20) Parkhutik, V. P.; Shershulsky, V. I. *J. Phys. D: Appl. Phys.* **1992**, *25*, 1258−1263.

(21) Patermarakis, G.; Moussoutzanis, K. *J. Electrochem. Soc.* **1995**, *142*, 737−743.

(22) Pan, H.; Lin, H. Y.; Feng, Y. P.; Gao, H. *IEEE Trans. Nanotechnol.* **2004**, *3*, 462−467.

(23) Garcia-Vergara, S. J.; Skeldon, P.; Thompson, G. E.; Habazaki, H. *Electrochim. Acta* **2006**, *52*, 681−687.

(24) Van Overmeere, Q.; Blaffart, F.; Proost, J. *Electrochem. Commun.* **2010**, *12*, 1174−1176.

(25) Lee, W.; Ji, R.; Gösele, U.; Nielsch, K. *Nat. Mater.* **2006**, *5*, 741−747.

(26) Csokan, P.; Sc, C. C. *Electroplat. Met. Finish.* **1962**, *15*, 75−82.

(27) Barberoglou, M.; Zorba, V.; Pagozidis, A.; Fotakis, C.; Stratakis, E. *Langmuir* **2010**, *26*, 13007−13014.

(28) Koch, K.; Barthlott, W. *Philos Trans. R. Soc. London, Ser. A* **2009**, *367*, 1487−1509.

(29) Onda, T.; Shibuichi, S.; Satoh, N.; Tsujii, K. *Langmuir* **1996**, *12*, 2125−2127.

(30) Neinhuis, C.; Barthlott, W. *Ann. Bot.* **1997**, *79*, 667−677.

(31) Bico, J.; Marzolin, C.; Quéré, D. *Europhys. Lett.* **1999**, *47*, 220−226.

(32) Boquet, L.; Lauga, E. *Nat. Mater.* **2011**, *10*, 334−337.

(33) Lee, W.; Park, B. G.; Kim, D. H.; Ahn, D. J.; Park, Y.; Lee, S. H.; Lee, K. B. *Langmuir* **2010**, *26*, 1412−1415.

(34) Ye, J.; Yin, Q.; Zhou, Y. *Thin Solid Films* **2009**, *517*, 6012−6015.

(35) Velleman, L.; Triani, G.; Evans, P. J.; Shapter, J. G.; Losic, D. *Microporous Mesoporous Mater.* **2009**, *126*, 87−94.

(36) Park, B. G.; Lee, W.; Kim, J. S.; Lee, K. B. *Colloid Surf., A* **2010**, *370*, 15−19.

(37) Mateo, J. N.; Kulkarni, S. S.; Das, L.; Bandyopadhyay, S.; Tepper, G. C.; Wynne, K. J.; Bandyopadhyay, S. *Nanotechnology* **2011**, *22*, 035703.

(38) Yao, L. J.; Zheng, M. J.; Ma, L.; Li, W.; Li, M.; Shen, W. Z. *Mater. Res. Bull.* **2011**, *46*, 1403−1408.

(39) Ran, C. B.; Ding, G. Q.; Liu, W. C.; Deng, Y.; Hou, W. T. *Langmuir* **2008**, *24*, 9952−9955.

(40) Sawitowski, T.; Beyer, N.; Wagener, S.; Schulz, F. *Nanotechnology* **2003**, *3*, 1−4.

(41) Kim, D.; Hwang, W.; Park, H. C.; Lee, K. H. *Curr. Appl. Phys.* **2008**, *8*, 770−773.

(42) Martín, J.; Mijangos, C. *Langmuir* **2009**, *25*, 1181−1187.

(43) Grimm, S.; Martín, J.; Rodriguez, G.; Fernández-Gutierrez, M.; Mathwig, K.; Wehrspohn, R. B.; Gösele, U.; Roman, J. S.; Mijangos, C.; Steinhart, M. *J. Mater. Chem.* **2010**, *20*, 3171−3177.

(44) Feng, X.; Mei, S.; Jin, Z. *Langmuir* **2011**, *27*, 14240−14247.

(45) Thieme, M.; Blank, C.; Pereira De Oliveira, A.; Worch, H.; Frenzel, R.; Höhne, S.; Simon, F.; Pryce Lewis, H. G.; White, A. J. Superhydrophobic Aluminum Surfaces: Preparation Routes, Properties and Artificial Weathering Impact. In *Contact Angle, Wettability and Adhesion*, Vol. *6*; Mittal, K. L., Ed.; Brill: Boston, MA, 2010; pp 251−268.

(46) Lazzara, T. D.; Kliesch, T.- T.; Janshoff, A.; Steinem, C. *ACS Appl. Mater. Interfaces* **2011**, *3*, 1068−1076.

(47) Nakamura, S.; Saito, M.; Huang, Li-F.; Miyagi, M.; Wada, K. *Jpn. J. Appl. Phys.* **1992**, *31*, 3589−3593.

(48) Chu, S. Z.; Wada, K.; Inoue, S.; Isogai, M.; Katsuta, Y.; Yasumori, A. *J. Electrochem. Soc.* **2006**, *153*, B384−B391.

(49) Bernardin, J. D.; Mudawar, I.; Christopher, R.; Walsh, C. B.; Franses, E. I. *Int. J. Heat Mass Transfer* **1997**, *40*, 1017−1033.
(50) Nielsch, K.; Choi, J.; Schwirn, K.; Wehrspohn, R. B.; Gösele, U. *Nano Lett.* **2002**, *2*, 677−680.
(51) Ono, S.; Masuko, N. *Corros. Sci.* **1992**, *33*, 503−507.
(52) Kant, K.; Low, S. P.; Marshal, A.; Shapter, J. G.; Losic, D. *ACS Appl. Mater. Interfaces* **2010**, *2*, 3447−3454.
(53) Rahmawan, Y.; Moon, M.- W.; Kim, K.- S.; Lee, K.- R.; Suh, K.- Y. *Langmuir* **2009**, *26*, 484−491.
(54) Adamson, A. W.; Gast, A. P. *Physical Chemistry of Surfaces*, 6th ed.; John Wiley & Sons: New York, 1997; Chapter II, Section 4.
(55) Zhong, R. Surface Wettability of Anodized Aluminum Oxides with Pore Sizes Larger than 200 nm. M.S. Thesis, KU Leuven, Belgium, June 2012.
(56) Bico, J.; Tordeux, C.; Quéré, D. *Europhys. Lett.* **2001**, *55*, 214−220.
(57) Feng, L.; Zhang, Y. A.; Xi, J. M.; Zhu, Y.; Wang, N.; Xia, F.; Jiang, L. *Langmuir* **2008**, *24*, 4114−4119.
(58) Ruan, M.; Li, W.; Wang, B. S.; Luo, Q.; Ma, F. M.; Yu, Z. L. *Appl. Surf. Sci.* **2012**, *258*, 7031−7035.